REPORT DOCUMENTATION PAGE

Form Approved
OMB No. 0704-01-0188

PLEASE DO NOT RETURN YOUR FORM TO THE ABOVE ADDRESS.

1. REPORT DATE *(DD-MM-YYYY)*	2. REPORT TYPE	3. DATES COVERED *(From - To)*
11-10-2008	REPRINT	

4. TITLE AND SUBTITLE
Two observed consequences of penetration electric fields

5a. CONTRACT NUMBER

5b. GRANT NUMBER

5c. PROGRAM ELEMENT NUMBER
62601F

6. AUTHORS
Cheryl Y. Huang
W. J. Burke*
C. S. Lin

5d. PROJECT NUMBER
2301

5e. TASK NUMBER
SD

5f. WORK UNIT NUMBER
A5

7. PERFORMING ORGANIZATION NAME(S) AND ADDRESS(ES)
Air Force Research Laboratory /RVBXP
29 Randolph Road
Hanscom AFB, MA 01731-3010

8. PERFORMING ORGANIZATION REPORT NUMBER
AFRL-RV-HA-TR-2010-1078

9. SPONSORING/MONITORING AGENCY NAME(S) AND ADDRESS(ES)

10. SPONSOR/MONITOR'S ACRONYM(S)
AFRL/RVBXR

11. SPONSOR/MONITOR'S REPORT NUMBER(S)

12. DISTRIBUTION/AVAILABILITY STATEMENT
Approved for public release; distribution unlimited.

13. SUPPLEMENTARY NOTES
Reprinted from: Journal of Atmospheric and Solar-Terrestrial Physics, 71, 2009 (1614-1622) © Elsevier, 2009
*Institute for Scientific Research, Boston College, Chestnut Hill, MA 02467

14. ABSTRACT
The influence of penetration electric fields (PEF) on storm-time energetic particles in the inner magnetosphere and on the stability of plasma in the low-latitude ionosphere is widely recognized. We describe two consequences of PEFs, regularly observed during magnetic storms that indicate their persistence throughout the main phases. These are (1) the presence of equatorial plasma bubbles (EPB) across the evening local time section during main phases and their absence throughout recovery, and (2) detections of low-energy ion precipitation in the dawn sector equatorward of the auroral electron boundary.

15. SUBJECT TERMS
Penetration electric fields; Magnetic storms; Low-latitude precipitation; Particle trajectories

16. SECURITY CLASSIFICATION OF:			17. LIMITATION OF ABSTRACT	18. NUMBER OF PAGES	19a. NAME OF RESPONSIBLE PERSON
a. REPORT	b. ABSTRACT	c. THIS PAGE			Cheryl Huang
UNCL	UNCL	UNCL	UNL	9	19B. TELEPHONE NUMBER *(Include area code)*

Journal of Atmospheric and Solar-Terrestrial Physics 71 (2009) 1614–1622

Contents lists available at ScienceDirect

Journal of Atmospheric and Solar-Terrestrial Physics

journal homepage: www.elsevier.com/locate/jastp

Two observed consequences of penetration electric fields

C.Y. Huang [a,*], W.J. Burke [a,b], C.S. Lin [a]

[a] Air Force Research Laboratory Space Vehicles Directorate, AFRL/RVBXP, 29 Randolph Road, Hanscom AFB, MA 01731-3010, USA
[b] Boston College Institute for Scientific Research, USA

ARTICLE INFO

Article history:
Accepted 3 September 2008
Available online 11 October 2008

Keywords:
Penetration electric fields
Magnetic storms
Low-latitude precipitation
Particle trajectories

ABSTRACT

The influence of penetration electric fields (PEF) on storm-time energetic particles in the inner magnetosphere and on the stability of plasma in the low-latitude ionosphere is widely recognized. We describe two consequences of PEFs, regularly observed during magnetic storms that indicate their persistence throughout the main phases. These are (1) the presence of equatorial plasma bubbles (EPB) across the evening local time sector during main phases and their absence throughout recovery, and (2) detections of low-energy ion precipitation in the dawn sector equatorward of the auroral electron boundary.

Published by Elsevier Ltd.

1. Introduction

This paper addresses two space environmental effects directly attributable to penetration electric fields (PEFs): (1) enhanced triggering of equatorial plasma bubbles (EPBs), and (2) altered magnetospheric particle trajectories. As a working definition we regard PEFs as the electric fields of magnetospheric origin that are commonly encountered at sub-auroral latitudes during the main phases of magnetic storms. PEFs and their effects have been observed with sensors on satellites in the ionosphere and inner magnetosphere as well as by ground-based radars.

EPBs exemplify a non-linear, generalized Rayleigh–Taylor (R–T) instability that evolves from bottomside plasma irregularities to burst through the F layer peak into the topside ionosphere (Ott, 1978). A simple understanding of their causality is obtained by considering the linear growth rate, γ, of the generalized R–T instability and the geophysical contexts in which it is realized (Scannapieco and Ossakow, 1976; Sultan, 1996).

$$\gamma \approx \frac{\Sigma_F}{\Sigma_F + \Sigma_E}\left[\frac{E \times B}{B^2} + U_n + \frac{g}{\nu^{eff}}\right]\frac{1}{N}\frac{\partial N}{\partial h} \quad (1)$$

where Σ_F and Σ_E are the conductances of the F- and E-layers, respectively, U_n is the downward neutral wind speed perpendicular to B, g is the local acceleration due to gravity at the equator, ν^{eff} is the effective, flux-tube integrated ion-neutral collision frequency, and $(1/N)(\partial N/\partial h)$ is the logarithmic density gradient. Under typical ionospheric conditions, growth periods, $1/\gamma$, are ~10 min (Basu, 1997). It takes several growth periods for large-amplitude irregularities to grow. Since g and B are constants at a given location, R–T growth rates are largely controlled by the variability of E, and the Σ_E/Σ_F ratio. The eastward electric fields required to drive the R–T instability in the dusk sector have three sources: (1) leakage of the solar quiet (Sq) current system into the nightside ionosphere (Eccles, 1998a, b), (2) electric field penetration from high to low latitudes (Nopper and Carovillano, 1978; Fejer and Scherliess, 1997), and (3) neutral winds associated with traveling atmospheric disturbances (TADs) and/or gravity waves (Hysell et al., 1990; Singh et al., 1997; McClure et al., 1998).

Huang et al. (2005) described a class of ion-precipitation events discovered during the storm main phase of the Halloween 2003 superstorm (29–31 October 2003). Particle sensors on DMSP satellites detected intense and sustained fluxes of keV ions precipitating in the morning sector up to 24° equatorward of the electron auroral boundary. Normally low-energy ions are forbidden access

* Corresponding author. Tel.: +1 781 377 1312; fax: +1 781 377 9950.
E-mail address: afrl.rvb.pa@hanscom.af.mil (C.Y. Huang).

1364-6826/$ - see front matter Published by Elsevier Ltd.
doi:10.1016/j.jastp.2008.09.018

to this region. A survey of the large DMSP database revealed that such events occur quite commonly during large magnetic storms. From the perspective of drift paths normally allowed to ions of plasma sheet origin, these DMSP observations were unexpected. Huang et al. (2005) also compared ion spectra simultaneously acquired by DMSP satellites in the ionosphere and by the Combined Release and Radiation Effects Satellite (CRRES) in the magnetosphere during the main phase of the magnetic storm on 24–25 March 1991. Indeed the DMSP F8 satellite also detected ion fluxes near dawn at sub-auroral latitudes with low-energy spectra similar to those observed during the October 2003 storm. The low-energy plasma analyzer (LEPA) on CRRES detected ion fluxes well earthward of the electron plasma sheet boundary at L shells conjugate to DMSP. An analysis of magnetospheric drift paths demonstrated that ions from the plasma sheet can access lower L shells near dawn than electrons only if penetration electric fields are both present and time varying. The trajectory calculations used electric fields measured by CRRES to drive a simple model of drift motions in the magnetosphere.

The paper is organized as follows: after a brief description of relevant satellite-borne sensors we provide observations of: (1) storm-time EPBs as evidence of PEF persistence, (2) characteristics of low-energy ion precipitation at low latitudes in the dawn sector during a large magnetic storm, and (3) spectral properties of ions on conjugate L shells in the inner magnetosphere. The final section uses a Volland–Stern model of electric fields in the equatorial plane as a tool for studying drift paths of test particles under the influence of time-varying PEFs. It should be noted that some of these results have been presented in earlier publications (Huang et al., 2002, 2005). In this paper, we unite high- and low-latitude phenomena previously reported, and emphasize the role of penetration electric fields in interpreting these results.

2. Instrumentation

DMSP satellites are three-axis stabilized spacecraft that fly in circular, Sun-synchronous, polar (inclination 98.7°) orbits at an altitude of ~840 km. The geographic local times of the orbits are either near the 1800–0600 (F8, F13), or 2100–0900 (F9, F15, F16) local time meridians. Offsets between the geographic and geomagnetic poles allow DMSP satellites to sample wide ranges of magnetic local times (MLT) over the course of a day. For DMSP satellites with flight designations 10 and higher, orbital ascending nodes are on the dusk side of the Earth. Thus, during the Halloween storm DMSP satellites moved toward the northwest (southeast) in the evening (morning) sector. Each satellite carried a suite of sensors to measure (1) fluxes of auroral electrons and ions [special sensor J4 or J5], (2) thermal plasma densities, temperatures, and drift motions [special sensor for ions electrons and scintillations, SSIES], and (3) magnetometers [special sensor for magnetic fields, SSM] to monitor field-aligned currents. Only DMSP satellites designated F12 and higher carry SSM. While this paper mostly concerns particle fluxes from J4 and/or J5 sensors, we also make use of potential distributions measured along DMSP trajectories.

Identical J4 sensors were mounted on the top surfaces of all DMSP satellites with flight designations F7–F15. They consist of two boxes each with cylindrical electrostatic analyzers (ESA) to measure the fluxes of downcoming electrons and ions with energies between 30 eV and 30 keV in 19 logarithmically spaced energy steps (Hardy et al., 1984). One ESA pair measures electron and ion fluxes from 30 eV to 1 keV; the second ESA pair covers the 1–30 keV range. A common energy step near 1 keV is used for cross calibration. Full ion and electron spectra are compiled every second.

The first J5 sensor was launched on DMSP F16 in October 2003, just prior to the onset of storm activity. J5 is a single triquadraspheric ESA that images incoming particles onto a microchannel plate. It also measures fluxes of ions and electrons in 19 logarithmically spaced energy steps from 30 eV to 30 keV each second. The main advance from J4 sensors is that the J5 measures particle fluxes in a 4° × 90° fan, ranging from zenith to the horizon. The 90° field-of-view is divided into six 15° angular sectors (Kadinsky-Cade et al., 2004). The sensor operates in two modes. Mode A operations emulate the performance characteristics of J4 sensors by summing counts from the six look sectors to accumulate one spectrum per second. In Mode B, a spectrum for each angular sector is accumulated every second. It thus takes 6 s to construct a full pitch-angle distribution.

The SSIES suite includes an ion trap to measure the total ion densities and an ion drift meter (IDM) to measure horizontal (V_H) and vertical (V_V) cross-track components of plasma drifts (Rich and Hairston, 1994). V_H and V_V are sampled six times per second but are normally reported as 4-s averages. They are then used to calculate the in-track component of electric field and the distribution of potential (Φ) along the trajectory. DMSP estimates of the polar cap potential (Φ_{PC}) are reported as differences between measured potential extrema in the Northern and Southern Hemispheres. Since trajectories usually do not cross potential maxima and minima, DMSP provides lower-bound estimates of the true Φ_{PC}.

CRRES was launched in July 1990 into an 18.2°-inclined eccentric orbit with an apogee at geocentric distance of 6.3 R_E and perigee at an altitude of 350 km. The orbital period was ~10 h. CRRES was spin stabilized at a rate of 2 rpm. Its spin axis always pointed within 15° of the Sun. The line of apsides precessed toward earlier local times at a rate of 0.67° per day. In March–June 1991 period, apogee moved through the evening to dusk MLT sector. Data used in this study were taken from LEPA (Hardy et al., 1993).

LEPA was a triquadraspheric ESA similar in concept to the J5 that measured fluxes of electrons and ions with energies between 10 eV and 30 keV. Fluxes at energies < 100 eV are unavailable. The ESAs had fields of view of 128° × 5.5° and were mounted on the spacecraft to cover the range 30°–150° with respect to the spin axis. The 128° field-of-view divided into 16 zones of 8° angular widths. Usually, the detectors sampled fluxes both parallel and antiparallel to the Earth's magnetic field (B) once per spin. The full energy range was swept 64 times per satellite

spin. Ideally, the detector thus sampled pitch angles from 0° to 180° every 15 s in a 5.5° × 8° solid angle. Data are displayed in an energy-versus-time format with a color code representing intensities. Fluxes detected within 30° of B, as measured by MFI, are separated according to whether the detector was looking toward the Earth or the magnetic equator. Fluxes outside this range of pitch angles are designated as perpendicular to B.

The EFI employed two 100 m tip-to-tip wire antennas as double probes with cylindrical and spherical sensors. We only use data acquired by the cylindrical probe at a rate of 32 samples per second. Two electric field components, approximately in the solar ecliptic Y and Z directions are calculated as least-squares fits to sine waves and calculated to produce one measurement per satellite spin.

3. Observations

In preparation for a comprehensive simulation of inner magnetospheric dynamics during the June 1991 magnetic storm by the Rice Convection Model (Garner et al., 2004) Burke et al. (1998) compared electric field distributions sampled by CRRES near the equatorial plane and by DMSP F8 near the dusk meridian in the ionosphere. The EFI on CRRES detected PEFs extending earthward of ring-current ions to $L \simeq 2$, where the spacecraft's $V \times B$ motion rendered environmental electric field measurements meaningless. Simultaneous IDM measurements from DMSP F8 in the ionosphere showed that during the main phase up to 60% of the evening cell potential appeared at sub-auroral latitudes. During the main phase of this and the July 1991 magnetic storm, DMSP F9 and F10 detected intense EPBs large depletions at early evening local times (Burke et al., 2000). Wilson et al. (2001) suggested that the observed storm-time EPBs were PEF effects.

In subsequent studies, Huang et al. (2001, 2002) found that EPBs occur during main phases of all magnetic storms, often at locations and seasons that deviate from the normal climatology (Gentile et al., 2006). During the recovery phase EPB activity is suppressed, often for several hours to days. Fig. 1 illustrates EPB occurrences (vertical dashed lines) and the Dst index (solid line) for 11 days in March 1991. Sharp decreases in Dst mark the main phase of a storm that started on day 83, with recovery beginning on day 84. The main-phase cluster of vertical lines indicates repeated observations of EPBs. By contrast, the recovery phase, which continued until day 88, is characterized by their noticeable absence.

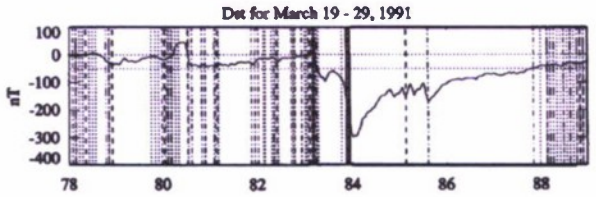

Fig. 1. Trace of the Dst index for 19–29 March 1991 interval that included a large magnetic storm. The vertical dash lines indicate detections of EPBs by DMSP satellite F10 and F9 in the evening sector near 20:00 and 21:00 LT, respectively.

Relevant to the present topic, we note that storm-time EPBs have deeper plasma depletions (Huang et al., 2001) and appear at earlier local times (Burke et al., 2004) than their quiet-time counterparts. Consideration of the growth rate, both observations indicate that main-phase growth rates are larger than during periods of magnetic quiet. During the magnetic storm on 10 November 2004, four polar-orbiting satellites, that were widely spread in local time, detected multiple and sustained EPB occurrences over the Pacific Ocean. In November, Σ_E/Σ_F ratios are relatively high in this longitude sector and EPBs are absent (Gentile et al., 2006). Since DMSP satellites move by ~25° in longitude from one ascending node to the next, each EPB encounter is with a different EPB-generation event. We thus regard these detections as evidence that PEFs must persist throughout the duration of a storm's main phase, triggering EPBs almost continuously, independent of its climatological probability.

Fig. 2 is a composite of DMSP F16 particle measurements compiled on 30 October 2003 that illustrates the second type of PEF effect. Data were acquired during a magnetic superstorm in which the minimum Dst exceeded −400 nT. From top to bottom the different plots show the number fluxes for electrons (solid lines) and ions (dotted lines) $(cm^2\,s\,sr)^{-1}$, average energy (keV), and the directional differential fluxes of downcoming electrons and ions $(cm^2\,s\,sr\,keV)^{-1}$. Auroral fluxes of plasma sheet origin, characterized by high-energy ions and somewhat cooler electrons, were seen until 01:47 UT. Electron fluxes cut off shortly before 01:48 UT (MLat = 52.8°). Equatorward of this boundary, ion fluxes of $\sim 10^8$ $(cm^2\,s\,sr)^{-1}$ persisted until 01:51 UT (MLat = 41°). The spectrogram shows that J5 sampled the most intense sub-auroral ion fluxes at $E < 100$ eV, but measurable fluxes appeared at $E > 10$ keV, (e.g. 01:50 UT; MLat = 46.6°). About 20 min prior to the F16 boundary crossing shown in Fig. 2, DMSP F13 (not shown) crossed the morning auroral electron boundary at MLat ≈ 52° near 07:00 MLT. The J4 sensor on F13 also detected intense, low-energy ion fluxes that extended to MLat = 40°. High-energy ions were not as strongly evident in F13 as in F16 observations.

Fig. 3 shows plots of IMF B_y and B_z (top), the cross-polar cap potential observed by DMSP satellites (middle), and the Sym-H (bottom) for the entire storm period. Plots in the top panel show hourly averaged values of the IMF B_Y (dash line) and B_Z (solid line) components measured by the Advanced Composition Explorer (ACE) satellite near the first Lagrangian point (L_1). Data are assigned to the universal times of acquisition. At the speeds reported by Skoug et al. (2004) it takes less than an hour for a solar-wind parcel to propagate from L_1 to Earth. Exact lag times are not critical for this report. Note three southward turnings leading to IMF B_Z minima of −14 and −24 nT near 08:00 and 19:00 UT on 29 October and −29 nT near 20:00 UT on 30 October.

The middle panel of Fig. 3 shows potentials measured by DMSP satellites F13 and F15 while crossing the morning (positive) and afternoon (negative) convection cells. The polar cap potential Φ_{PC} is estimated as the difference between the positive and negative extrema

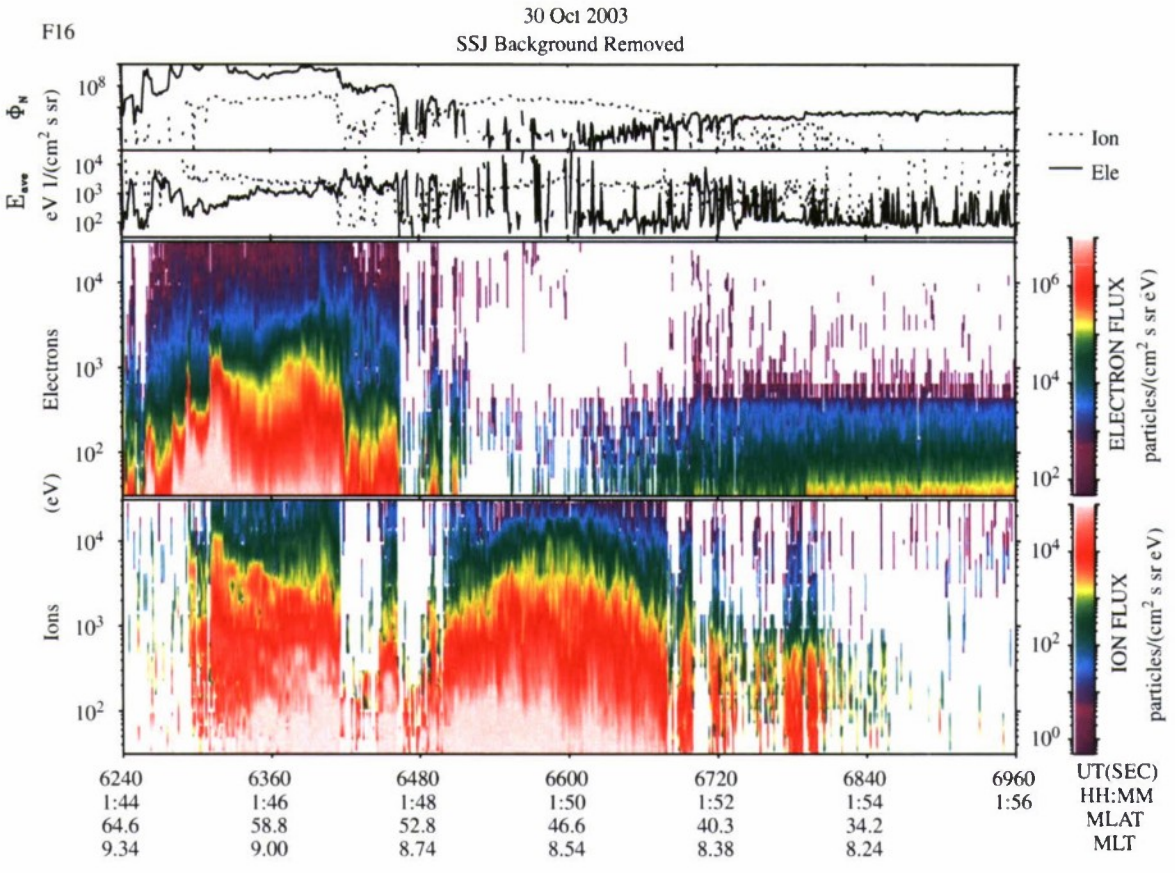

Fig. 2. DMSP F16 spectrogram with an example of the low-energy ion precipitation during the Hallaween storm. The top two panels show number and average energy flux for ions and electrons, the bottom two panels show the fluxes of both species. Ion fluxes extend between 01:48 and 01:52 UT, ~12° equatorward of the auroral electron boundary.

measured by DMSP. During individual passes DMSP satellites sample some indeterminate fractions of the entire potential in the afternoon and morning cells. The envelope of DMSP measurements thus provides lower-bound estimates of the electric potential that the interplanetary medium imposes on the magnetosphere and the high-latitude ionosphere. Assuming that the potential in both cells is roughly equal, the second and third southward IMF turnings produced Φ_{PC} maxima that approached 300 kV.

The bottom panel of Fig. 3 shows the Sym-H index for the storm period, obtained from the World Data Center, Kyoto (http://swdcwww.kugi.kyoto-u.ac.jp/index.html). We display the 1-min Sym-H index rather than Dst because of its higher temporal resolution. The first sudden commencement occurred on 29 October at ~06:15 UT; Dst reached −200 nT by 08:00 UT. A partial recovery was followed by an intensification of activity beginning near 15:00 UT. This enhancement ended on 30 October at ~00:30 UT when Sym-H reached −378 nT. The third enhancement began at 17:45 UT, with Sym-H decreasing to −400 nT by 21:10 UT. During this storm Sym-H/Dst minima lagged Φ_{PC} maxima by a few hours. Solid bars at the bottom of Fig. 3 indicate periods when DMSP satellites detected intense fluxes of low-energy ions. These intervals roughly coincide with the minima in Sym-H.

Equatorward boundaries of ion and electron precipitation observed between 18:00 UT on 29 October and 06:00 UT on 30 October are shown in Fig. 4. Plotted observations represent DMSP F13 and F16 boundary encounters in both Southern and Northern Hemispheres. Hollow and solid symbols depict electron and ion boundaries, respectively. The average equatorward cutoffs for ion and electron precipitation during the interval occurred at ~39° and 52°, respectively. The average separation was 13°; the maximum of 24° occurred early on 30 October, nearly coincident with the Sym-H minimum.

To provide a context for understanding these and similar observations from DMSP we turn to CRRES measurements during the magnetic superstorm of March 1991. During this storm CRRES orbital paths were favorable for examining ion fluxes at low L shells near dawn, with apogee and perigee near 21:30 and 09:30 MLT, respectively. Fig. 5 contains spectrograms of electron and ion directional differential fluxes acquired by LEPA during a full orbit from 14:00 to 24:00 UT on 24 March. Spectra are presented in groups of three that from top to bottom indicate fluxes at pitch angles near 90°, 0° and 180°, respectively. Shortly after 15:00 UT (17:50 MLT) while the satellite was moving outbound, it crossed a ring-current nose structure (Smith and Hoffman, 1974) seen in

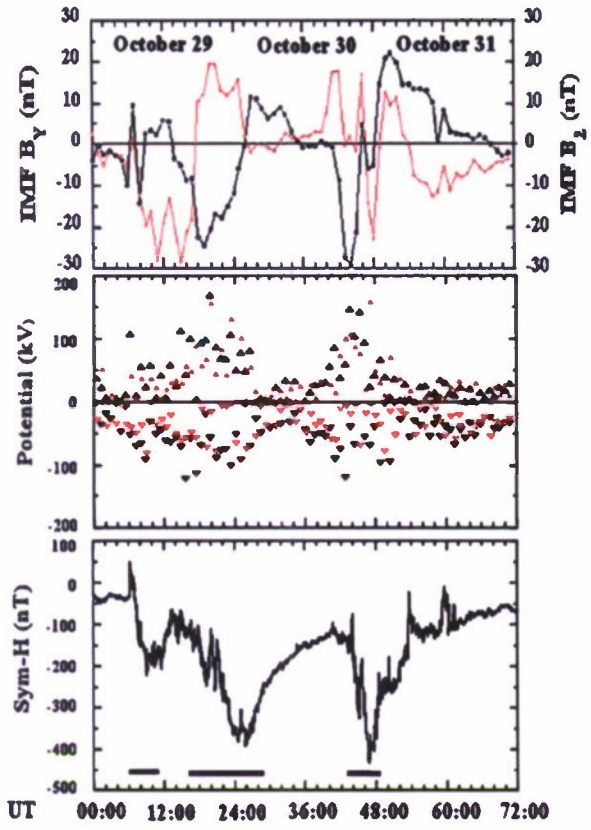

Fig. 3. Geophysical parameters observed during the storm of 29–31 October 2003. The top panel shows IMF B_Y (red) and B_Z (black) measured near the L1 point by ACE. The second panel gives potential extrema measured in the morning (positive) and evening (negative) convection cells by DMSP F13 (black) and F15 (black). The bottom panel contains a plot of the Sym-H index. The heavy bars indicates periods of sub-auroral ion precipitation in the morning sector.

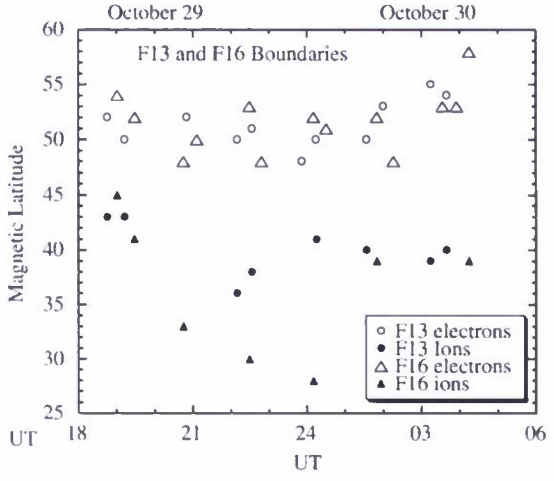

Fig. 4. The boundaries of auroral electron (hollow symbols) and ion (solid symbols) precipitation as measured by DMSP F13 (circles) and F16 (triangles) during the second period of the storm, from 18 UT on 29 October to 6 UT on 30 October 2003.

two lower ion panels. In both cases a population of low-energy ions ($E<1$ keV) is also seen. These spectral structures are signatures of ion conics generated in the conjugate ionosphere (Rubin et al., 1995). On the inbound pass near the end of 24 March, CRRES crossed four geophysically significant boundaries. Each boundary encounter is listed in UT and satellite coordinates (radial distance in R_E, MLat, MLT, and ILat)

(1) 22:50 UT (3.7, −17.7°, 0.67, 61.7°), fluxes of ions and electrons intensified with energies of several keV as CRRES entered the plasma sheet from the lobe;
(2) 23:20 UT (2.37, −23.7°, 2.48, 53.7°), electron fluxes cut off at the Earthward edge of the plasma sheet;
(3) 23:35 UT (1.76, −25.2°, 3.96, 46°), most intense fluxes of <1 keV ions;
(4) after 23:40 UT (1.56, −24.8°, 4.7, 41.9°), no measurable fluxes.

In this case the region of sub-auroral ion precipitation in the pre-dawn sector spanned the ILat range 41.9°–46.2°. DMSP crossed the equatorward boundary of auroral electron precipitation at 53.7°. These are close to the average locations of boundary encounters by DMSP satellites during the October 2003 storm (Fig. 4).

4. Discussion

4.1. Equatorial plasma bubbles

Eq. (1) shows that the growth of the generalized R–T instability from small plasma density irregularities in the bottomside into full blown depletions at topside altitudes is largely controlled by the variability of E, and the Σ_E/Σ_F ratio. As indicated above the total electric field is a superposition of contributions from many sources. The generation of quiet time EPBs reflects contributions of the ever-present dayside dynamo and the consequent Sq current system. Vertical plasma drifts at the magnetic equator associated with Sq currents typically have two maxima, one near noon and the other near dusk. The latter, referred to as a pre-reversal enhancement is followed by a rapid descent of the ionosphere by ~20:00 LT as the zonal component of the local electric fields turns from eastward to westward (Scherliess and Fejer, 1999).

Eq. (1) indicates that γ is enhanced when E has an eastward component and the ionospheric E-layer vanishes so that $\Sigma_E \rightarrow 0$. Thus there is a finite window for EPB generation that starts when a flux tube passes into darkness and ends when the electric field reverses. A comparison of the local times at which ROCSAT and DMSP detect EPBs showed that during magnetically quiet times they were only detected after 20:00 LT and during disturbed times after 19:30 LT (Burke et al., 2004). We ascribe this to the presence of electric fields generated by the interplanetary medium. Nishida (1968) provided the first experimental evidence for PEFs causing the equatorial electrojet to intensify and relax as the interplanetary magnetic field (IMF) swung from northward to southward

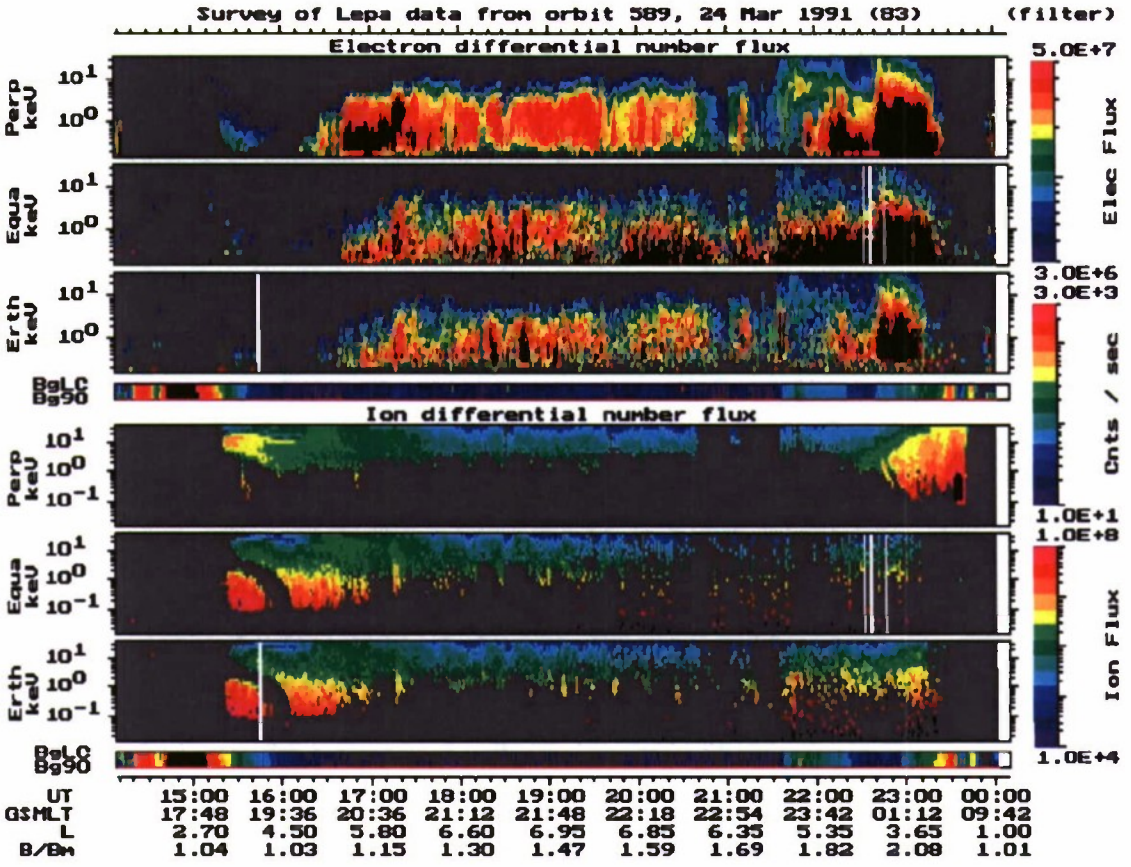

Fig. 5. Directional differential fluxes measured by LEPA on CRRES between 14:00 and 24:00 UT on 24 March 1991. The top three panels show electron fluxes in three look directions; ion fluxes are similarly displayed in bottom three panels. For both species the top, middle and bottom spectrograms indicate fluxes perpendicular to B, along B looking toward the magnetic equator, and along B looking toward Earth, respectively.

and back. He argued that the IMF modulates the intensity of the global DP 2 currents associated with large-scale convection patterns. Striking confirmation of IMF control was recently provided by Kelley et al. (2003). The most important contributions of DMSP measurement to understanding of IMF control is that during the main phase of magnetic storms PEFs constitutes the dominant E-field source and they last, with low shielding, for hours rather than for a few tens of minutes.

Even during solar minimum, when storms are much weaker, most of the EPBs that reach DMSP altitude tend to occur during downturns in Dst. During the solar minimum years 1995–1997, an average of 34% of the DMSP detections of EPBs occurred in periods when $(\partial(\mathrm{Dst})/\partial t)$ declined by at least 5 nT/h for over 2 h. Thus during solar minimum, even small PEFs may play a large contributing role in generation of EPBs.

The second storm-time effect observed by DMSP is the repeated absence of EPB detections during recovery phases. We tentatively ascribe this effect to the disturbance dynamo. Blanc and Richmond (1980) suggested that storm-time heating of the nightside ionosphere–thermosphere generates a dynamo whose polarity is opposite to that of its dayside counterpart. Their overall effect would be reduce or reverse the suppression of EPBs during storm recovery. It remains unclear how a disturbance dynamo can operate effectively suppressing normal effects of the dayside dynamo for the several days of storm-time recovery.

4.2. Low-latitude ion precipitation

Detections of low-energy ions precipitating from the inner magnetosphere near the dawn meridian lead to several questions: What is their source? How did they drift to low L shells in the morning sector? What allowed the observed separation between electron and ion boundaries to develop at these local times? In order to address these questions we considered the forces in the magnetosphere that act on test particles and their affect on drift trajectories.

Because of its analytic simplicity we choose the Volland–Stern (V–S) (Volland, 1973; Stern, 1975; Ejiri, 1978; Burke, 2007) model that was developed as a conceptual tool for estimating the guiding-center trajectories of ions and electrons in the inner magnetosphere. V–S operates in inertial coordinates in the equatorial plane, with the magnetic field B represented as a rotating dipole with a superposed dawn-to-dusk electric field E. Guiding centers of test particles are subject to $E \times B$ and magnetic-gradient drifts, conserving their total energy

and magnetic moments $\mu = mv_{\perp}^2/B$. The symbols m and $v_{\perp}$ represent a particle's mass and velocity component perpendicular to B, respectively.

We divide ions into three classes, (1) $\mu < \mu_c$, (2) $\mu \approx \mu_c$, and (3) $\mu > \mu_c$. The critical magnetic moment μ_c is defined as the value of μ for which the westward gradient-curvature drift V_G exactly matches its eastward corotation drift V_C in the midnight sector just outside the zero-energy Alfvén boundary (ZEAB). Ejiri (1978) showed that at this east–west stagnation point μ_c ions can only drift toward the Earth under the influence of the dawn-to-duck electric field. Inside the ZEAB magnetic-gradient forces dominate over corotation and μ_c ions drift into the dusk sector. Near the dusk meridian they have the apex energy of nose structures found in ion spectrograms (Smith and Hoffman, 1974).

The guiding centers of test particles of the first class drift close to equipotential lines. The V–S model identifies two equipotential topologies in the equatorial plane of the magnetosphere, called opened and closed. Open equipotentials begin at the reconnection line in the magnetotail and end on the dayside magnetopause. The region close to Earth is dominated by corotation, where equipotential lines close on themselves. The location of the separatrix between the two topologies is the ZEAB. Its location and shape depend on the potential imposed on the magnetosphere by the solar wind and the degree of shielding provided by Region 2 field-aligned currents (Harel et al., 1981). The ZEAB moves closer to Earth during storms when Φ_{PC} is large. Under steady-state conditions charged particles of either polarity with $\mu \approx 0$ are confined to regions inside or outside the ZEAB. Thus, the guiding centers of test particles of the first class essentially drift close to equipotential lines. Here we consider the drift paths of charge particles during large magnetic storms, by adapting the V–S model to consider time-varying electric fields with different degrees of shielding.

Fig. 6 shows the magnetospheric mapping of the equatorward boundary of auroral electron precipitation derived from DMSP measurements during periods of high magnetic activity by Gussenhoven et al. (1981). The boundary's line of symmetry is directed toward dusk but is rotated into the late afternoon sector (1991). Huang et al. (2005) found that this boundary shape was consistent with locations of CRRES crossings into and out of the plasma sheet as monitored by LEPA. We began calculations of all ion and electron drift paths outside of this boundary and let them move under the influence of an imposed and corotation electric fields as well as magnetic-gradient forces. The imposed electric field was oriented in the dawn-to-dusk direction with magnitudes of 0.5 and 2.6 mV/m. These correspond to field values measured by EFI at ~1518–1640 and ~2250–2340 UT on 25 March 1991, respectively.

Fig. 6 also shows the drift paths of selected test particles, ions on the left, electrons on the right. For clarity drift path for each species was separated by μ as follows: $0 < \mu < \mu_c$ (top); $0.8\,\mu_c < \mu < 1.2\mu_c$ (middle); $1.2\mu_c < \mu < 2\mu_c$ (bottom). The value of μ_c estimated from LEPA measurements at ~15:40 UT was 14.2 eV/nT, corresponding to a ring-current energy of 10 keV and a magnetic field

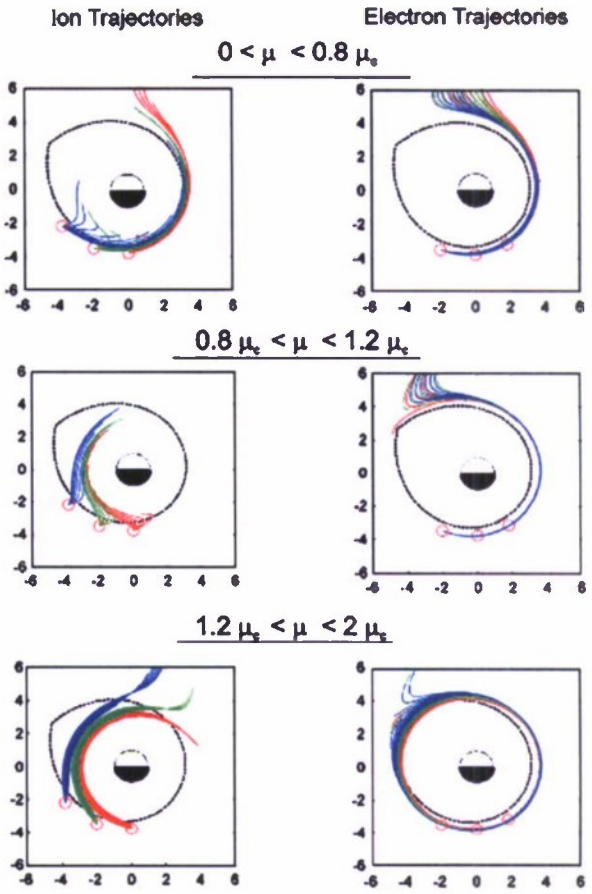

Fig. 6. Ion and electron trajectories with a constant uniform dawn-to-dusk electric field $E_0 = 0.5$ mV/m. Ion trajectories are shown in the left three panels, and electron trajectories are presented in the right panels for three different ranges of magnetic moment μ. In each panel particle trajectories from three different initial points are represented in three colors. Ion trajectories are shown for three initial points: 20:00, 22:00 and 24:00 h LT at 4.3 R_E, whereas electron trajectories are shown for three initial points: 22:00, 24:00 and 02:00 h LT at 4.3 R_E. Eight trajectories are plotted from each initial point for particles with magnetic moments evenly separated by $0.1\mu_c$ in the range appropriate for the various panels.

strength of 735 nT. Test ion (electron) injection points were at 4.3 R_E and 20:00, 22:00, 24:00 (22:00, 24:00, 02:00) LT, about 0.5 R_E beyond the mapped auroral electron boundary. The resulting trajectories shown in Fig. 7 are differentiated by color according to initial position.

Most ions with $\mu < \mu_c$ drift toward dawn. Only a few trajectories significantly cross the auroral boundary. Ions with $\mu \approx \mu_c$ penetrate most closely to the Earth on the dusk side. All ions with $\mu > \mu_c$ drift toward dusk, just Earthward of the auroral boundary. Because their corotation and gradient drifts have the same sense, all electrons move toward dawn and generally remain near or beyond the boundary. Ions with $\mu < \mu_c$ reaching the dawn sector show little radial separation from electrons. Varying the electric field strengths did not produce marked qualitative differences in the resulting drift paths.

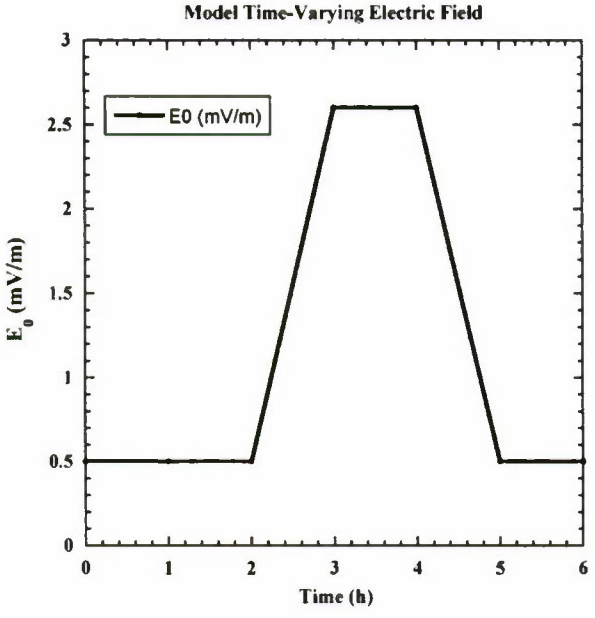

Fig. 7. Temporal variation of the dawn-to-dusk electric field E_0 used for calculating particle trajectories during the dynamic phase.

We next considered affects of time-varying electric fields. In qualitative agreement with CRRES measurements, Fig. 7 shows the background electric field increasing smoothly from 0.5 to 2.6 mV/m over a half hour. It held this value for an hour before returning to its initial state. We also assumed that no shielding occurred during the period of interest. Fig. 8 show the effects of applying this time-varying and unshielded electric field. The symbol and color scheme have the same format as Fig. 6. In this case, ion trajectories for all values of μ penetrate significantly closer to Earth at dawn and morning local times than electrons. Note too that most ions with $\mu < \mu_c$ drift directly to the dawn sector; ions with $\mu \geq \mu_c$ reach the dawn after wrapping around the dayside.

5. Conclusions

We have presented two specific examples of phenomena directly arising from PEFs. First, EPBs during magnetic storms are triggered by the total electric field of which the PEF can be large or even dominant. During quieter intervals, the generation of EPBs is enhanced by the presence of a PEF even when a storm does not result.

A second consequence of PEFs is the alteration of ion drift paths during storms in which the electric field varies in time. Our simple modeling of ion and electron trajectories demonstrates that particle drifts can be separated by large distances under the influence of a time-varying PEF, giving rise to precipitation of ions well equatorward of the electron auroral boundary.

Both of these effects are common occurrences during storms. EPBs are a regular feature of storm main phase, and low-latitude ion precipitation is observed in all large ($Dst < -150$ nT) storms lasting more than a few hours.

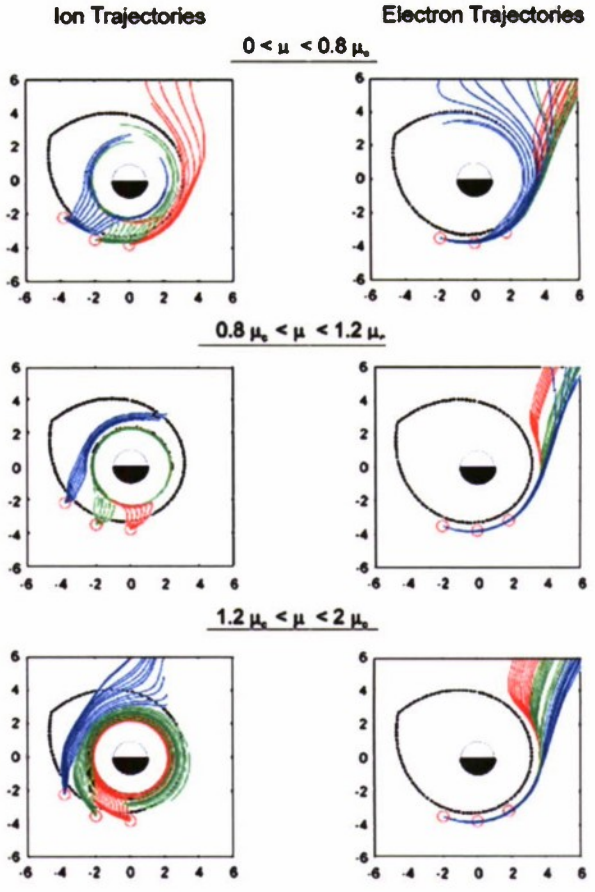

Fig. 8. Ion and electron trajectories with the time varying dawn-to-dusk electric field given in Fig. 7. Trajectories are presented in the same format as Fig. 6.

Relatively simple modeling reveals that PEFs are the underlying cause in both types of phenomena.

Acknowledgments

Support for the presented work was provided by the Air Force Office of Scientific Research, Task 2311SDA3, and AF Contracts FA8718-04-C-0055 and FA8718-08-C-0012 with Boston College.

References

Basu, B., 1997. Generalized Rayleigh–Taylor instability in the presence of time-dependent equilibrium. Journal of Geophysical Research 102, 17,305.

Blanc, M., Richmond, A.D., 1980. The ionospheric disturbance dynamo. Journal of Geophysical Research 85, 1669.

Burke, W.J., 2007. Penetration electric fields: a Volland–Stern approach. Journal of Atmospheric and Solar-Terrestrial Physics 69, 1114.

Burke, W.J., Maynard, N.C., Hagan, M.P., Wolf, R.A., Wilson, G.R., Gentile, L.C., Gussenhoven, M.S., Huang, C.Y., Garner, T.W., Rich, F.J., 1998. Electrodynamics of the inner magnetosphere observed in the dusk sector by CRRES and DMSP during the magnetic storm of June 4–6, 1991. Journal of Geophysical Research 103, 29,399.

Burke, W.J., Rubin, A.G., Maynard, N.C., Gentile, L.C., Sultan, P.J., Rich, F.J., de La Beaujardière, O., Huang, C.Y., Wilson, G.R., 2000. Ionospheric disturbances observed by DMSP at middle to low latitudes during

the magnetic storm of June 4–6, 1991. Journal of Geophysical Research 105, 18391.
Burke, W.J., Gentile, L.C., Huang, C.Y., Valladares, C.E., Su, S.Y., 2004. Longitudinal variability of equatorial plasma bubbles observed by DMSP and ROCSAT-1. Journal of Geophysical Research 109 (A12301).
Eccles, J.V., 1998a. A simple model of low-latitude electric fields. Journal of Geophysical Research 103, 26,699.
Eccles, J.V., 1998b. Modeling investigation of the evening prereversal enhancement of the zonal latitude electric field in the equatorial ionosphere. Journal of Geophysical Research 103, 26,709.
Ejiri, M., 1978. Trajectory traces of charged particles in the magnetosphere. Journal of Geophysical Research 83, 4798.
Fejer, B.G., Scherliess, L., 1997. Empirical models of storm time equatorial zonal electric fields. Journal of Geophysical Research 102, 24,047.
Garner, T.W., Wolf, R.A., Spiro, R.W., Burke, W.J., Fejer, B.G., Sazykin, S., Roeder, J.L., Hairston, M.R., 2004. Magnetospheric electric fields and plasma sheet injection to low L-shells during the June 4–5 1991 magnetic storm: comparison between the rice convection model and observations. Journal of Geophysical Research 109, A02214.
Gentile, L.C., Burke, W.J., Rich, F.J., 2006. A climatology of equatorial plasma bubbles from DMSP 1989–2004. Radio Science 41, RS5S21.
Gussenhoven, M.S., Hardy, D.A., Burke, W.J., 1981. DMSP F2 electron observations of equatorward auroral boundaries and their relationship to magnetospheric electric fields. Journal of Geophysical Research 86, 768.
Hardy, D.A., Schmidt, L.K., Gussenhoven, M.S., Marshall, F.J., Yeh, H.C., Shumaker, T.L., Huber, A., Pantazis, J., 1984. Precipitating electron and ion detectors (SSJ/4) for block 5D/Flights 4–10 DMSP satellites: calibration and data presentation, Technical Report, AFGL-TR-84-0317, Air Force Geophysical Laboratory, Hanscom AF8, MA.
Hardy, D.A., Walton, D.W., Johnstone, A.D., Gough, M.P., Huber, A., Pantazis, J., Burkhardt, R., 1993. The low energy plasma analyzer. IEEE Transactions on Nuclear Science 40, 246.
Harel, M., Wolf, R.A., Spiro, R.W., Reiff, P.H., Chen, C.-K., Burke, W.J., Rich, F.J., Smiddy, M., 1981. Quantitative simulation of a magnetospheric substorm, 2. Comparison with observations. Journal of Geophysical Research 86, 2242.
Huang, C.Y., Burke, W.J., Machuzak, J.S., Gentile, L.C., Sultan, P.J., 2001. DMSP observations of equatorial plasma bubbles in the topside ionosphere near solar maximum. Journal of Geophysical Research 106, 8131.
Huang, C.Y., Burke, W.J., Machuzak, J.S., Gentile, L.C., Sultan, P.J., 2002. Equatorial plasma bubbles observed by DMSP satellites during a full solar cycle: toward a global climatology. Journal of Geophysical Research 107 (A12), 1434.
Huang, C.Y., Burke, W.J., Lin, C.S., 2005. Ion precipitation in the dawn sector during geomagnetic storms. Journal of Geophysical Research 110, A11213.
Hysell, D.L., Kelley, M.C., Swartz, W.E., Woodman, R.F., 1990. Seeding and layering of equatorial spread F by gravity waves. Journal of Geophysical Research 95, 17,253.
Kadinsky-Cade, K., Holeman, E.G., McGarrity, J., Rich, F.J., Denig, W.F., Burke, W.J., Hardy, D.A., 2004. First results from the SSJS precipitating particle sensor on DMSP F16: simultaneous observation of keV and MeV particles during the 2003 halloween storms. Eos Transaction AGU 85 (1) (Joint Assembly Suppl., Abstract SH53A-03).
Kelley, M.C., Makela, J.J., Chau, J.L., Nicholls, M.J., 2003. Penetration of the solar wind electric field into the magnetosphere/ionosphere system. Geophysical Research Letters 30 (4), 1158.
McClure, J.P., Singh, S., Bamgboye, D.K., Johnson, F.S., Kil, H., 1998. Occurrence of equatorial F region irregularities: evidence for tropospheric seeding. Journal of Geophysical Research 103, 29,119.
Nishida, A., 1968. Coherence of geomagnetic DP2 magnetic fluctuations with interplanetary magnetic variations. Journal of Geophysical Research 73, 5549.
Nopper, R.W., Carovillano, R.L., 1978. Polar–equatorial coupling during magnetically active periods. Geophysical Research Letters 5, 699.
Ott, E., 1978. Theory of Rayleigh–Taylor bubbles in the equatorial ionosphere. Journal of Geophysical Research 83, 2066.
Rich, F.J., Hairston, M., 1994. Large-scale convection patterns observed by DMSP. Journal of Geophysical Research 99, 3827.
Rubin, A.G., Burke, W.J., Hardy, D.A., 1995. Low-energy ion spectral peaks detected by CRRES in the plasma sheet. Journal of Geophysical Research 100, 19,221.
Scannapieco, A.J., Ossakow, S.L., 1976. Nonlinear equatorial spread F. Geophysical Research Letters 3, 451.
Scherliess, L., Fejer, B.G., 1999. Radar and satellite global equatorial F region vertical drift model. Journal of Geophysical Research 104, 6829.
Singh, S., Johnson, F.S., Power, R.A., 1997. Gravity wave seeding of equatorial plasma bubbles. Journal of Geophysical Research 102, 7399.
Skoug, R.M., Gosling, J.T., Steinberg, J.T., McComas, D.J., Smith, C.W., Ness, N.F., Hu, Q., Burlaga, L.F., 2004. Extremely high solar wind speed: 29–30 October 2003. Journal of Geophysical Research 109, A09102.
Smith, P.H., Hoffman, R.A., 1974. Direct observations in the dusk hours of the characteristics of the storm time ring current particles during the beginning of magnetic storms. Journal of Geophysical Research 79, 966.
Stern, D.P., 1975. The motion of a proton in the equatorial magnetosphere. Journal of Geophysical Research 80, 595.
Sultan, P.J., 1996. Linear theory and modeling of the Rayleigh–Taylor instability leading to the occurrence of equatorial spread F. Journal of Geophysical Research 101, 26,875.
Volland, H., 1973. A semiempirical model of large-scale magnetospheric electric fields. Journal of Geophysical Research 78, 171.
Wilson, G.R., Burke, W.J., Maynard, N.C., Huang, C.Y., Singer, H.J., 2001. Global electrodynamics observed during the initial and main phases of the July 1991 magnetic storm. Journal of Geophysical Research 106, 24,517.